Bio-Design and Manufacturing (2022) 5:451–464
https://doi.org/10.1007/s42242-022-00190-7

RESEARCH ARTICLE

Customizable design of multiple-biomolecule delivery platform for enhanced osteogenic responses via 'tailored assembly system'

Hyun Lee[1,2] · Min-Kyu Lee[3,4] · Ginam Han[1,2] · Hyoun-Ee Kim[3,5] · Juha Song[6] · Yuhyeon Na[1,2] · Chang-Bun Yoon[7] · SeKwon Oh[8] · Tae-Sik Jang[9] · Hyun-Do Jung[1,2]

Received: 1 September 2021 / Accepted: 6 February 2022 / Published online: 24 March 2022

Abstract

Porous titanium (Ti) scaffolds have been extensively utilized as bone substitute scaffolds due to their superior biocompatibility and excellent mechanical properties. However, naturally formed TiO_2 on the surface limits fast osseointegration. Different biomolecules have been widely utilized to overcome this issue; however, homogeneous porous Ti scaffolds could not simultaneously deliver multiple biomolecules that have different release behaviors. In this study, functionally graded porous Ti scaffolds (FGPTs) with dense inner and porous outer parts were fabricated using a two-body combination and densification procedure. FGPTs with growth factor (BMP-2) and antibiotics (TCH) exhibited suitable mechanical properties as bone substituting material and presented good structural stability. The release of BMP-2 was considerably prolonged, whereas the release of TCH was comparable to that of homogenous porous titanium scaffolds (control group). The osteogenic differentiation obtained using FGPTs was maintained due to the prolonged release of BMP-2. The antimicrobial properties of these scaffolds were verified using *S. aureus* in terms of prior release time. In addition, various candidates for graded porous Ti scaffolds with altered pore characteristics were presented.

✉ Tae-Sik Jang
tsjang@chosun.ac.kr

✉ Hyun-Do Jung
hdjung@catholic.ac.kr

1 Department of Biomedical-Chemical Engineering, Catholic University of Korea, Bucheon 14662, Republic of Korea

2 Department of Biotechnology, The Catholic University of Korea, Bucheon 14662, Republic of Korea

3 Department of Materials Science and Engineering, Seoul National University, Seoul 08826, Republic of Korea

4 Querrey Simpson Institute for Bioelectronics, Northwestern University, Evanston, IL 60208, USA

5 Biomedical Implant Convergence Research Center, Advanced Institutes of Convergence Technology, Suwon 443-270, Republic of Korea

6 School of Chemical and Biomedical Engineering, Nanyang Technological University, 70 Nanyang Drive, Singapore 637457, Singapore

7 Department of Advanced Materials Engineering, Korea Polytechnic University, Siheung-si, Gyeonggi-do 15073, Republic of Korea

8 Surface R&D Group, Korea Institute of Industrial Technology, Incheon 21999, Republic of Korea

9 Department of Materials Science and Engineering, Chosun University, Gwangju 61452, Republic of Korea

Graphic abstract

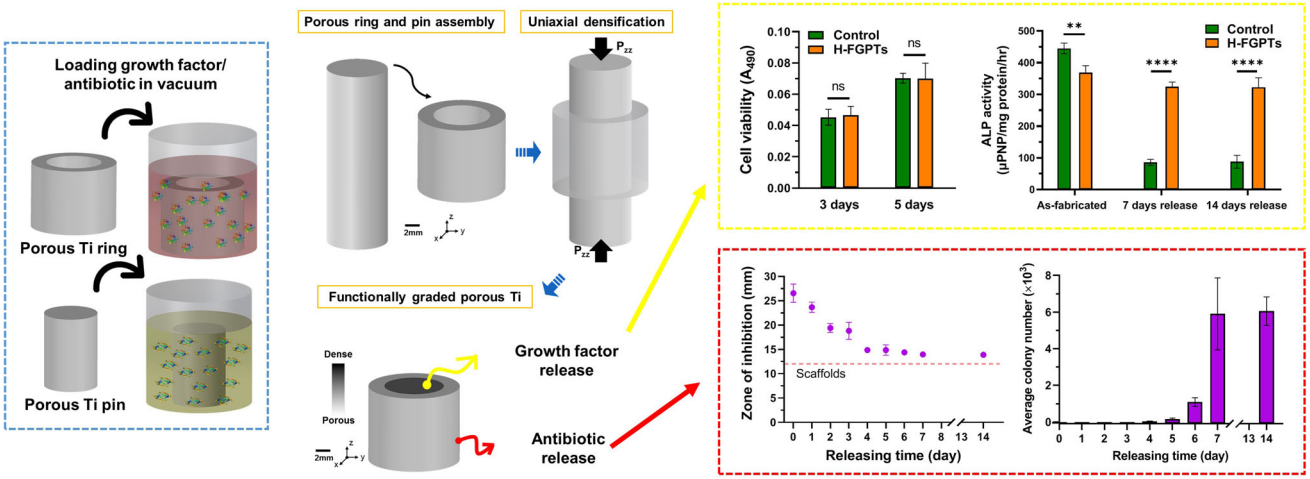

Keywords Functionally graded porous titanium scaffold · Tailored assembly system · Mechanical tunability · Multiple-biomolecule delivery · Bone tissue engineering

Introduction

In the past decades, a variety of metallic materials were utilized as artificial replacements at sites with malfunctioned bones, which could not provide sufficient support to applied loads [1–5]. Meanwhile, titanium (Ti) and its alloys have been extensively applied as bone grafts due to their excellent mechanical properties, biocompatibility, and chemical stability [6–11]. However, there are still challenges to satisfy clinical applications such as poor bone to Ti integration and the risk of bacterial infections. For example, despite the biocompatibility of Ti, naturally formed TiO_2 on a pristine Ti bone graft surface has been regarded as a bioinert ceramic due to the difficulty observed in the formation of a direct chemical bond with living bone tissues. Consequently, a long osseointegration period (approximately 3–4 months) is normally required [12, 13]. In order to overcome this issue, a number of surface treating methods were investigated in recent studies to enhance the biocompatibility of such metallic scaffolds [14–17].

A common strategy for improving bioactivity is the application of biomolecules, including growth factors [18, 19], drugs [20, 21], peptides [22, 23], and genetic materials [24–26], which can be delivered through bone grafts. Bone grafts with a localized biomolecule delivery system can enhance the efficacy of the released biomolecules compared to oral ingestion or inoculation. Moreover, these grafts reduce the need for multiple surgical interventions, and more biomolecules than one are often loaded into them. In the context of orthopedic surgery, antibiotics should be released from the bone graft in the initial stage after surgery in order to reduce acute inflammation in the tissue [27, 28], whereas growth factors such as bone morphogenetic protein-2 (BMP-2) should be provided via a relatively prolonged release system to make the bone regeneration process more efficient [29, 30]. For bone defects arising from traces of removed bone tumor, there is a need for a biomolecule delivery platform that can provide effective chemoprevention of the growth of bone tumor cells while simultaneously endowing the bone grafts with osteogenic capability to generate new bone tissue. Moreover, both angiogenesis and osteogenesis are crucial during the process of bone repair because neovascularization allows for the transportation of essential ingredients to the defect site [31, 32]. Therefore, advanced therapeutic systems aim to provide the simultaneous delivery of multiple growth factors for stimulating both angiogenesis and osteogenesis.

Another issue related to Ti-based bone graft failure is the stress-shielding phenomenon resulting from the mismatch of elastic modulus between natural bone and graft, consequently leading to bone resorption by deficient load transfer [33–37]. In terms of solving the problem of poor interlocking between bone and graft, adopting a porous structure has been one of the most promising strategies [38–42]. By decreasing the elastic modulus with the increased porosity of Ti graft, the above undesirable phenomenon can be circumvented. Additionally, enhanced differentiation of osteoblastic cells and enlarged contact sites of cells could be achieved by roughening the pore surface [43–47]. However, the introduction of a porous structure in a metallic biomaterial can lead to undesir-

able mechanical properties; for example, the implant stiffness may not be suitable for bone defect sites. Furthermore, parts for sufficient mechanical sustentation and those efficiently delivering biomolecules should be constructionally integrated within a single bone implant. As the parameters of porous structure are improved to satisfy biological requirements, the mechanical properties become insufficient for use as a bone substitute. However, if the mechanical properties are adjusted to eliminate the stress-shielding effect, the porous structure will not satisfy the requirements of cells or tissues in patients.

In our previous work, we demonstrated that the densification procedure provided a biomimetic titanium scaffold (BTS) with mechanical tunability, enabling a variety of applications ranging from highly porous fillers to dense load-bearing implants [48, 49]. Moreover, we showed that the enhanced bioactivity obtained via the scaffold densification procedure allowed for sustainable release due to the excellent pore interconnectivity and relatively high surface area with controllable tortuosity. Thus, we hypothesized that multi-layered porous structures with varying mechanical properties and multiple-biomolecule release behaviors could be customized by this tailored assembly system, with the constructed scaffolds providing a new design for bone-repairing platforms.

In this study, an efficient fabrication method of a multiple-biomolecule delivery platform is implemented, which is composed of two parts with distinctive pore characteristics using a tailored assembly system. After arranging the two parts with different sizes, they were assembled into a single scaffold by compressing through the z-axis, resulting in hierarchically graded porous structure [48]. Especially for the proposed assembly system, two dissimilar biomolecules could be loaded individually but released concurrently. Tetracycline hydrochloride (TCH) and bone morphogenetic protein (BMP-2) were, respectively, chosen as antibiotics and growth factor to be loaded into the scaffold. As antibiotics should be released faster than growth factors to repress initial inflammation, antibiotics were loaded into the porous parts while growth factors were loaded into the denser parts for more sustained release. The structure and pore characteristics of the constructed Ti scaffolds with graded porous structure were investigated by scanning electron microscopy (SEM) and micro-computed tomography (micro-CT). The compressive features of the scaffolds were also assessed by compression testing. The release behavior of rhBMP-2 and TCH was monitored by UV–Vis spectroscopy, and in vitro antimicrobial and biocompatibility tests were also performed.

Materials and methods

Dynamic freeze casting to produce porous Ti scaffolds

Mixtures containing 15 vol%, 20 vol%, and 25 vol% Ti were prepared by blending pure Ti powder (325 mesh, Alfa Aesar, Ward Hill, MA, USA), camphene ($C_{10}H_{16}$, Sigma Aldrich, St. Louis, MO, USA) as a pore forming agent, and 1 wt.% oligomeric polyester (HypermerKD-4, UniQema, Everberg, Belgium) as a dispersant to produce porous Ti scaffolds with 70%, 60%, and 50% of porosity. Ti mixtures were placed in an aluminum mold with 60 mm diameter and 60 mm height, and then heated at 60 °C and rotated at a speed of 30 r/min to fully melt the camphene. Subsequently, the mold was cooled down to 44 °C with identical rotation speed, and it was kept in this state for 24 h to obtain solidified green bodies. After 24 h of solidification, the green bodies were closely packed by a cold isostatic press (CIP) process at 200 MPa for 5 min, and they were further frozen at −80 °C. The fully frozen green bodies were freeze-dried to sublimate the camphene. The treated green bodies were heated at a rate of 5 °C/min in a vacuum furnace until reaching 1300 °C and maintained at this temperature for 2 h.

Preparation of homogeneous and graded porous Ti scaffolds

The produced 50% and 70% porous Ti scaffolds were processed to specific diameter and height as noted in Table 1. Prior to assembly, any possible exterior contamination by the electro-discharge machining process was removed through submersion of the scaffolds in 70% HNO3 for 1 h. Especially, the scaffolds that were utilized in drug release, antimicrobial testing, and in vitro cell testing were sterilized through immersion in 70% EtOH, autoclaving, and UV irradiation. For structural and mechanical evaluation, ring- and pin-shaped porous Ti scaffolds (70% porosity) were put together to form a single functionally graded porous Ti scaffold (FGPTs) through pressing along the z-axis to interlock the two types of scaffolds. A total of L-FGPTs and H-FGPTs were fabricated to demonstrate two types of FGPTs with low and high degree of difference between the pore characteristics of the outer and the inner parts. The intended architecture of the FGPTs was fabricated through the combination of ring parts with 70% porosity and densified pin parts with eventual 50% and 30% porosity by applying a strain value of 0.40 and 0.57, respectively. To prepare specimens for the drug release test, porous Ti scaffolds with 50% of porosity and H-FGPTs were chosen as the control group and experimental group, respectively. The ring-shaped porous Ti components

Table 1 The initial size of ring and pin parts for fabricating functionally graded porous Ti scaffolds

Group	Evaluation	Height (mm)		Diameter (mm)	
Non-graded					
70%	Mechanical properties	10		12	
60%	Mechanical properties	10		12	
50%	Mechanical properties	10		12	
	In vitro tests	5			
		Ring	Pin	Ring	Pin
Graded structure					
L-FGPTs	Mechanical properties	10	16.7	D_{out}:12 D_{in}: 8.7	8.5
H-FGPTs	Mechanical properties	10	23.3	D_{out}:12 D_{in}: 8.7	8.5
	In vitro tests	5	11.6	D_{out}:12 D_{in}: 8.7	8.5

were immersed in 100 μg/mL TCH solution, while the pin-shaped porous Ti components and porous Ti scaffolds used as controls were immersed in 10 μg/mL BMP-2 solution. These were also kept in an evacuated state for 30 min to fully infiltrate the solutions into the pores. After immersion, the scaffolds were stabilized in a sterilized state. The adsorption efficiency of rhBMP-2 was (23.0 ± 0.7)% and the TCH was (33.2 ± 2.3)%. The BMP-2-loaded specimens for the control group were then loaded with TCH followed by an identical procedure. The same procedure was followed to prepare the scaffolds for in vitro biological tests with 10 μg/mL of BMP-2 and 11.8 μg/mL TCH for the control groups, and 6.5 μg/mL of BMP-2 and 16.9 μg/mL of TCH for H-FGPTs. The reason for utilizing different concentrations for the control group and the H-FGPTs was based on the pore volume in each group. To prevent contamination, each step was followed by a washing and drying process on a clean bench.

Structural evaluation

A dimensional approach was used when calculating the porosity of scaffolds. The porosity (P) was computed from the density of the samples following the below equation:

$$P = 100 \times \left(1 - \frac{m_s/V_s}{\rho_{Ti}}\right),$$

where m_s represents the sample mass, V_s the sample volume, and ρ_{Ti} the theoretical density of Ti (4.51 g/cc).

The surface structure of scaffolds was observed using SEM (JSM-5600, JEOL Techniques, Tokyo, Japan), and the three-dimensional inner structure was analyzed by micro-CT (Skyscan 1173 X-ray m-tomography System, Skyscan, Kontich, Belgium).

Assessment of compressive properties

The compressive strength and stiffness of the prepared specimens (diameter = 12 mm, height = 10 mm, $N = 3$) were measured utilizing a load frame (Instron 5582, Instron Corp., Canton, MA, USA) at 1 mm/min loading speed. In the case of H-FGPTs, a push-out test was conducted to confirm the failure stress using specimens with 12 mm in diameter and 5 mm in height ($N = 3$). In addition, a cyclic compression loading test was performed by compressing and releasing each sample for 20 times at a rate of 1 mm/min until reaching 1% strain and 110 MPa, which are similar to the representative yield strain and longitudinal yield stress of the human cortical bone [50].

In vitro release behavior of BMP-2 and TCH

The release of BMP-2 (Cellumed, Korea) and TCH (Aldrich, USA) from the scaffolds was tracked at pre-determined time points by examination and simultaneous evaluation through UV–Vis spectrophotometry (UV-1700, Shimadzu, Japan) after being fully submerged in 3 mL of Dulbecco's phosphate-buffered saline (DPBS). The wavelengths chosen to measure the absorbance of BMP-2 and TCH were 195 nm and 360 nm, respectively.

In vitro analysis of biocompatibility and antimicrobial effect

The specimens used in both tests measured 12 mm in diameter and 5 mm in height. MC3T3-E1 cells (ATCC, CRL-2593, Rockville, MD, USA) were cultured separately on samples with each specific density for different usages. 5×10^4, 3×10^4, and 0.2×10^4 cells/mL were cultivated on the samples for attachment, proliferation, and differen-

tiation tests, respectively, in minimum essential medium (α-MEM, Welgene Co., Ltd., Korea) containing 10% fetal bovine serum (Life Technologies, Inc., USA) and 1% antibiotics (100 U/mL penicillin and 100 μg/mL streptomycin, GIBCO, Grand Island, NY, USA) in a humidified incubator with 5% CO_2 at 37 °C. The shapes of cells were observed by confocal laser scanning microscopy (CLSM, Fluoview FV1000, Olympus, Japan) after 1 day of culture. The cells attached on the scaffolds were sequentially treated using 4% paraformaldehyde, 0.1% Triton X-100, and 1% bovine serum albumin prior to the staining procedure. The cell staining procedure was followed using phalloidin (colored in red) for the cytoskeleton and DAPI (colored in blue) for the nuclei. The daily exchange of culture medium to prevent the accumulation of TCH was performed before the proliferation test. After day 3 and 5 of culture, the cell viability was observed by MTS assay (CellTiter 96 Aqueous One Solution, Promega, USA). The absorbance of the medium was evaluated at 490 nm wavelength using a microplate reader (Model 550, Biorad, USA) followed by allowing 2 h of reaction time. To assess the degree of differentiation via alkaline phosphatase (ALP) activity assay, the remaining BMP-2 and TCH on the arranged scaffolds were extracted by 7 and 14 days of immersion in DPBS in an incubator under 5% CO_2 at 37 °C. The extraction process was then followed by cell culturing along with the scaffolds. After 1 day of culture, the medium was refreshed using culture medium containing 10 mM β-GP and 50 mg/mL ascorbic acid. The medium was replaced every 3 days throughout the 13 days of cell culture. Absorbance was measured at 405 nm using a microplate reader and the values were converted into ALP activity based on a standard curve.

An antimicrobial test was performed using *S. aureus* (ATCC 6538, Rockville, USA). In order to obtain a seed culture, 50 μL of bacterial suspension was cultured for 15 h after being injected into 3 mL of fresh Luria–Bertani (LB) broth (BD DifcoTM, 244,620, USA). A volume of 200 μL *S. aureus* suspension was injected into 15 mL of LB broth after being cultured at 37 °C while shaking at 200 r/min. After the injections, the two types of samples were spread on separate LB agar plates and holes of 11.5 mm in diameter were made where the specimens were located. The prepared scaffolds and *S. aureus* were preserved in an incubator for 1 day to monitor the inhibition zone. To observe the formation of colonies, inoculation of *S. aureus* suspension (1.3×10^7 CFU/mL) was performed on the sterilized samples followed by 1 day of culture. Subsequently, the samples were rinsed by DPBS twice and placed in 15-mL tubes containing 3 mL of DPBS. All of adhered bacteria were torn off from the samples by severe vortex shaking. Viable bacteria in the DPBS were then diluted and spread on a LB agar plate. After 1 day of incubation at 37 °C, individual colonies were observed and their numbers were counted.

Statistical analysis

All experimental results were expressed as mean ± standard deviation. Normality was evaluated by Shapiro–Wilk test and statistical significance was determined through Student's T test. A p value of less than 0.05 was considered as statistically significant.

Results

Structural evaluation

The schematic diagram presenting the fabrication method of functionally graded porous titanium scaffold with different biomolecules is demonstrated in Fig. 1. The ring-shaped parts

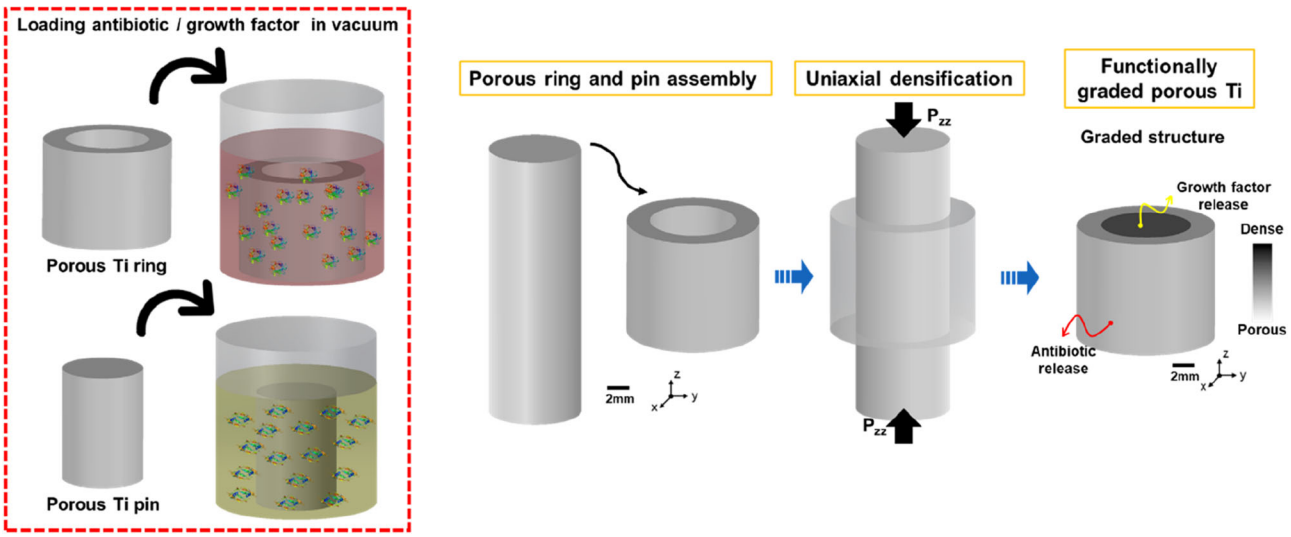

Fig. 1 Schematic illustration of functionally gradient porous titanium (Ti) scaffold fabrication with dual drug loading

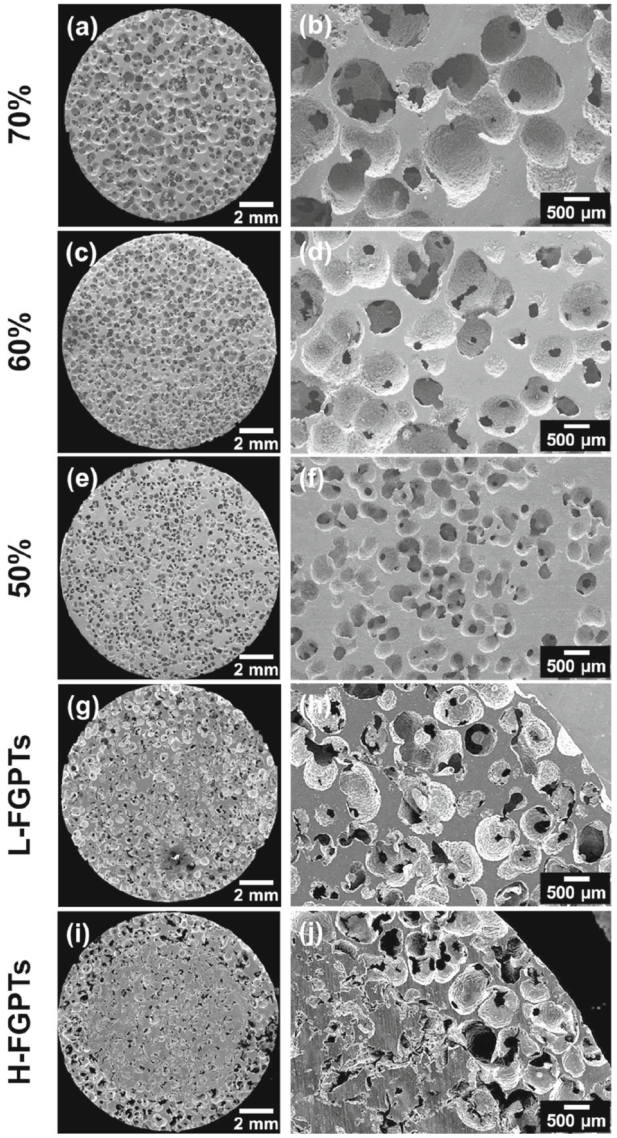

Fig. 2 Representative scanning electron microscopy (SEM) images of produced porous titanium scaffolds at low and high magnification. (**a**, **b**) 70% porosity; (**c**, **d**) 60% porosity; (**e**, **f**) 50% porosity; (**g**, **h**) L-FGPTs, and (**i**, **j**) H-FGPTs

containing TCH and the pin-shaped parts containing rhBMP-2 were prepared separately. The amount of strain was set as 0.40 and 0.57, respectively, to achieve 50% and 30% of final porosity from the initial 70% following the equation suggested in the literature [48]:

$$P = 100 \times \left(1 - \frac{0.3}{1-\varepsilon}\right),$$

where P represents the final porosity of the scaffold and ε the strain applied to the scaffold.

Figure 2 demonstrates the representative surface structure of the fabricated scaffolds. As illustrated in Figs. 2a–2f, spherical pores with even distribution were created in the Ti scaffolds with controlled porosities of 70% (Figs. 2a and 2b), 60% (Figs. 2c and 2d), and 50% (Figs. 2e and 2f), which are similar to those of previous articles [9, 48, 49]. The scaffolds featured decreasing pore size along with increasing initial Ti contents. On the other hand, different pore characteristics (porosity and pore size) between the pin and ring parts were observed in the fabricated functionally graded porous Ti scaffolds. The outer parts of functionally graded porous Ti scaffolds were composed of spherical pores while deformed pores were observed in the densified inner parts. As shown in Figs. 2g and 2h, a discrete layer between ring- and pin-shaped parts was observed in L-FGPTs, which contained densified 50% pin-shaped parts. Compared to L-FGPTs, H-FGPTs exhibited a more dramatic structural difference between the two parts (Figs. 2i and 2j).

The interior pore characteristics of the scaffolds were additionally evaluated by micro-CT. Figure 3a illustrates cross-sectional images by the horizontal and vertical axis. Uniformly distributed spherical pores could be observed in the scaffolds with 70%, 60%, and 50% of porosity. On the other hand, L-FGPTs and H-FGPTs exhibited hierarchically distributed pores in terms of pore shape and pore size. Especially for vertical cross-sectional images of functionally graded porous Ti scaffolds, the pore shapes were similar in inner parts, which indicated homogeneous densification along the z-axis. The pore size distribution is illustrated in Fig. 3b, which matched well with the reconstructed micro-CT images. Typical bell-shaped distributions were observed in homogeneously porous Ti scaffolds, while broadened distributions with two slight peaks were shown in FGPTs. The quantified porosity values following decreasing porosities of 70%, 60%, and 50% were (72 ± 2)%, (60 ± 2)%, and (49 ± 2)%, respectively. The overall porosity of L-FGPTs was (61 ± 1)% with (52 ± 1)% for inner and (70 ± 2)% for outer parts. Compared to L-FGPTs, H-FGPTs exhibited an overall porosity of (50 ± 2)% with (32 ± 1)% for inner and (69 ± 1)% for outer parts. The calculated pore sizes of the produced porous Ti scaffolds were different at 426 ± 99 μm (15 vol%), 355 ± 76 μm (20 vol%), and 274 ± 63 μm (25 vol%). The pore size of each part in functionally graded porous Ti scaffolds was 242 ± 91 μm for inner parts and 374 ± 107 μm for outer parts in L-FGPTs. On the other hand, each part of H-FGPTs possessed 105 ± 55 μm for inner parts and 372 ± 101 μm for outer parts.

Compressive properties of functionally graded porous titanium scaffolds

The compressive properties of homogenous porous Ti scaffolds and FGPTs were assessed. The homogeneous porous Ti scaffolds (50% to 70%) and L-FGPTs exhibited the repre-

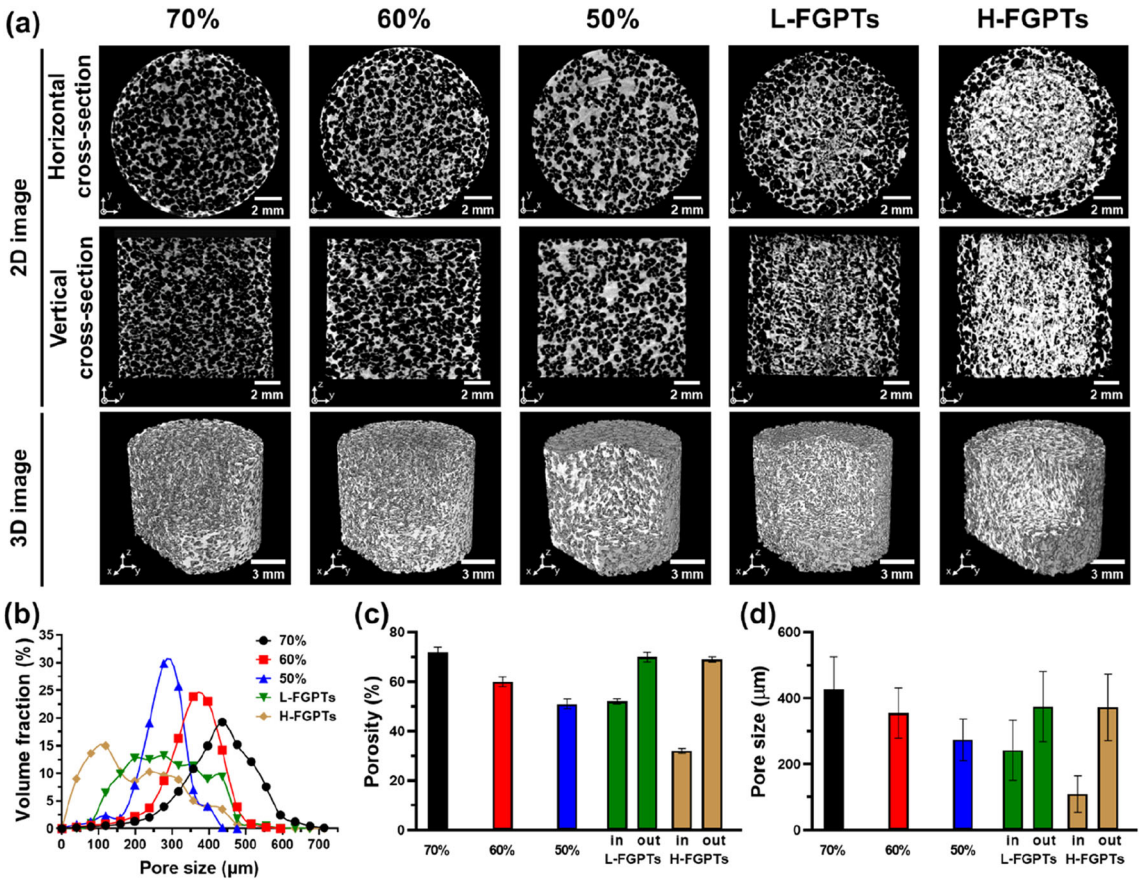

Fig. 3 **a** 2D cross-sectional and 3D reconstructed micro-CT images; **b** pore size distribution, **c** porosity, and **d** average pore size of the produced porous Ti scaffolds

sentative stress–strain curves of porous scaffolds, consisting of a linear elastic region, a plateau region, and a densification region with continuously increasing compressive stress following increasing strain (Fig. 4a). However, H-FGPTs exhibited a decreasing trend after the yield point, and the densification region appeared after it reached the minimum stress point around 124 MPa, as shown in Fig. 4a. The computed yield compressive strength and stiffness values are summarized in Fig. 4b. The yield compressive strength and stiffness were proportional to the initial Ti contents, which were, respectively, 57.8 ± 2.9 MPa and 3.9 ± 0.3 GPa for 15 vol% Ti and 166.7 ± 11.2 MPa and 16.7 ± 0.3 GPa for 25 vol% Ti. However, the functionally graded porous Ti scaffolds exhibited different behaviors compared to homogeneously porous Ti scaffolds. Even though the yield compressive strength followed the trend between porosity and strength, the trend of stiffness did not follow the porosity change. After comparing the mechanical properties and the possible utility of functionally graded structure, further experiments were conducted focusing on porous Ti scaffolds with 50% of porosity and H-FGPTs. Figures 4c and 4d demonstrate the results of cyclic compression tests of H-FGPTs under constraints with 1% strain and 110 MPa compressive stress based on the mechanical properties of cortical bone [50]. For 20 cycles, identical stress–strain curves were obtained at 1% strain condition, while slightly shifted stress–strain curves were obtained at 110 MPa condition. The maximum failure stress was also evaluated by measuring the load required to detach the ring and pin parts, and the obtained failure stress was 69.3 ± 5.9 MPa.

Release behavior of BMP-2 and TCH from functionally graded porous Ti scaffolds

The release behaviors of BMP-2 and TCH were monitored for 56 d in DPBS while comparing two groups of prepared scaffolds. In case of BMP-2, loaded BMP-2 was mostly released within 7 d for scaffolds of the control group, whereas significantly prolonged release behavior was obtained for H-FGPTs, as illustrated in Fig. 5a. On the other hand, the release profile of TCH was similar between the control group and H-FGPTs (Fig. 5b). Prolonged release behavior was shown for H-FGPTs in comparison with the control group. The observed release behavior was plot-

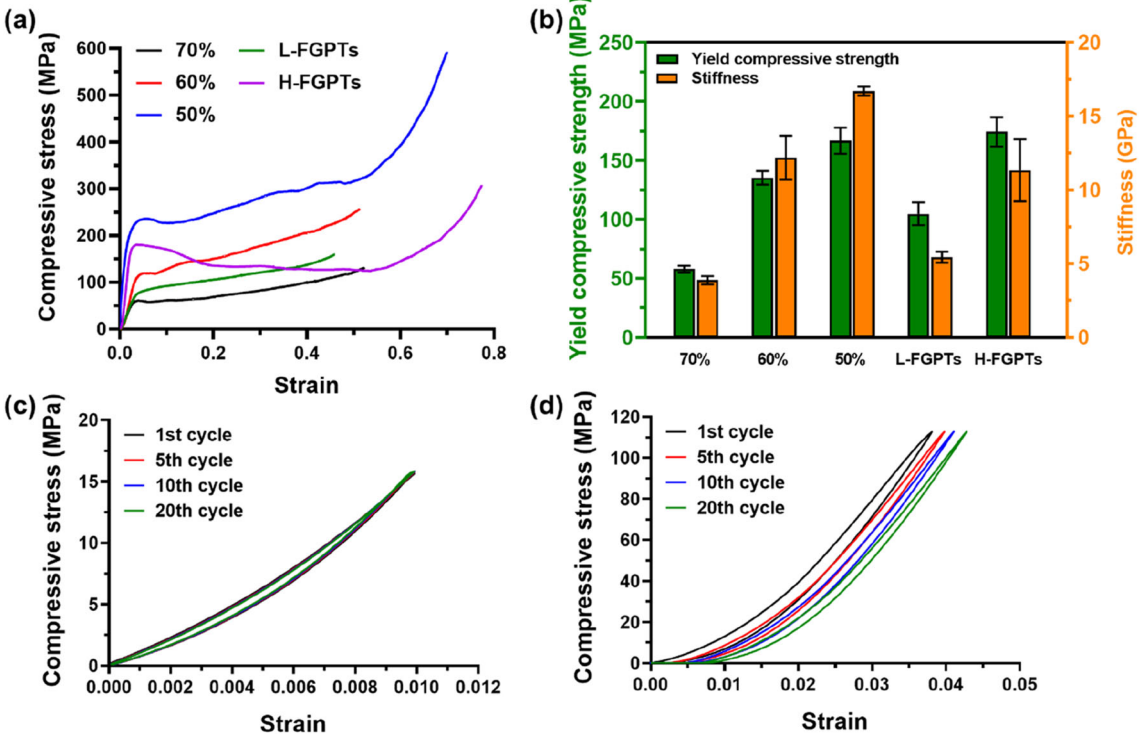

Fig. 4 **a** Stress–strain curve and **b** quantified yield compressive strength and stiffness of each scaffold. Monitoring of cyclic compression loading of H-FGPTs under the constraint of **c** 1% strain and **d** 110 MPa compressive stress

ted in first-order kinetics; the rate constant (k) was largely different for BMP-2 release and it was similar for TCH release between the control and FGPTs. Based on the release profile, the relative tortuosity factors were calculated and their differences were only considerable for BMP-2 release.

In vitro biocompatibility tests

The initial attachment of preosteoblast cells was evaluated by CLSM. As shown in Fig. 6a, the regions were classified into ring and pin parts for H-FGPTs. All of the cells were well attached onto the scaffolds regardless of regions with the different biomolecules of BMP-2 and TCH. Cell viability after 3 d and 5 d of culturing was monitored while refreshing the medium every day to avoid the accumulation of antibiotics. The degree of proliferation was similar between the control group and H-FGPTs both at 3 d and 5 d of culturing (Fig. 6b). However, ALP activity was considerably different at each determined precedent releasing time, as illustrated in Fig. 6c. At the initial stage, ALP activity was higher for the control group than that for the H-FGPTs. However, after 7 days of release, ALP activity dramatically decreased in the control group while it was sustained in the H-FGPTs. As demonstrated in Fig. 5a, almost all of BMP-2 was released within 7 days in the control group, whereas certain amounts of BMP-2 were still left inside the H-FGPTs.

In vitro antimicrobial tests

The monitoring of inhibition zone at determined time intervals and colony formation test were carried out using *S. aureus*, which is frequently found in the surgical infection site [51]. Scaffolds with different immersion times were placed onto the agar plate containing *S. aureus*. After 1 d of incubation, a clear inhibition zone was observed after prior immersion time of 3 days, and *S. aureus* covered nearly all of the scaffolds after 4 days of prior immersion (Fig. 7a). The diameter of inhibition zone was calculated based on the optical images, and a gradually decreasing trend was obtained (Fig. 7b). A similar result was acquired in the colony formation test as shown in Fig. 7c. A colony emerged from the scaffolds after 4 days of immersion, the number of colonies dramatically increased from 5 to 7 days, and they saturated by 14 days (Fig. 7d). Increasing the time while infections are reduced is possible with a higher dose of TCH, but this should be carefully considered since it can kill nearby cells, which is a common phenomenon in research related to antibacterial agents [52, 53].

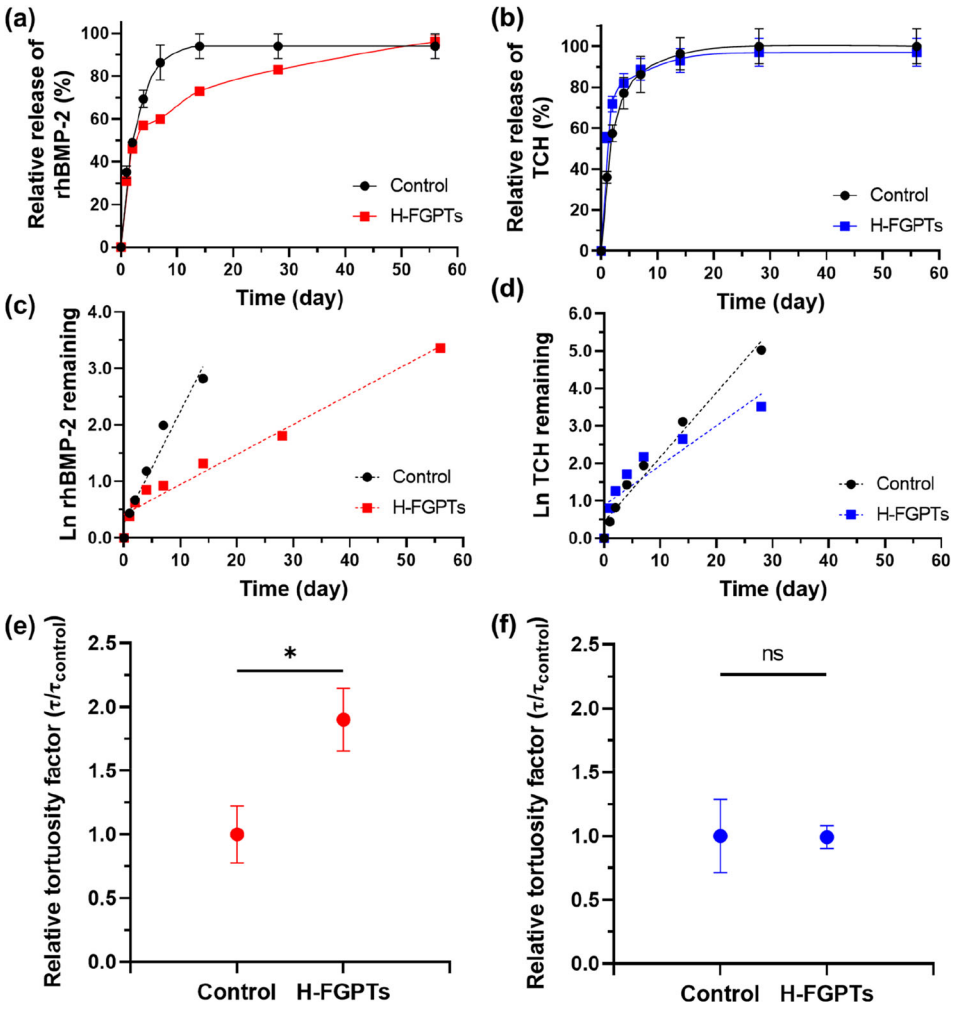

Fig. 5 Relative release, transformed first-order kinetics, and calculated relative tortuosity factor of (**a**, **c**, and **e**) BMP-2 and (**b**, **d**, and **f**) TCH for the control and H-FGPTs (*$p < 0.05$)

Discussion

In our previous work, we demonstrated the biomimetic structure of porous Ti scaffolds with dense outer structure [54]. Enlightened by that research, revised inversely structured functionally graded porous Ti scaffolds were constructed in this paper for faster bone infiltration to the scaffolds, which would result in a higher degree of fixation between scaffold and bone. Scaffolds with 50% to 70% of porosity were firstly prepared as initial scaffolds for densification along with comparative groups of L-FGPTs and H-FGPTs. Interfaces in L-FGPTs were more notable than those in H-FGPTs, which was due to less interlocking between the ring- and pin-shaped parts. In further analysis using micro-CT, the obtained porosity of each part showed good accordance with the proven theoretical calculation formula proposed in the former article, which evidenced the well-conducted homogeneous densification [48]. The obtained hierarchical structure is useful for facilitating interlocking between the scaffold and surrounding bone, since new bone would be regenerated inside the pores with full connection to the original bone. In addition to the aspect of tissue regeneration, the inner dense part could act as a load-bearing part enduring the applied loads.

Comparing the mechanical properties of L-FGPTs and H-FGPTs to homogeneous porous Ti scaffolds with similar porosity, they presented reduced stiffness that is beneficial to alleviate the stress-shielding effect. This phenomenon is attributed by deficient interfaces at the joint of inner and outer parts when compared to homogeneous porous scaffolds with fully sintered particles in the pore walls. However, the yield compressive strength of L-FGPTs was considerably lower than that of porous Ti scaffolds with 60% of porosity, whereas H-FGPTs exhibited yield compressive strength comparable to that of porous Ti scaffolds with 50% of porosity, structural stability, and the possibility for them to be utilized as bone substituting scaffolds. Even though the stress–strain curves under 110 MPa shifted as the number of cycles increased, the degree of shifting per cycle was reduced. To address the structural stability of H-FGPTs, failure stress was measured by push-out test. The measured failure stress between ring and pin parts of H-FGPTs was sevenfold higher than that

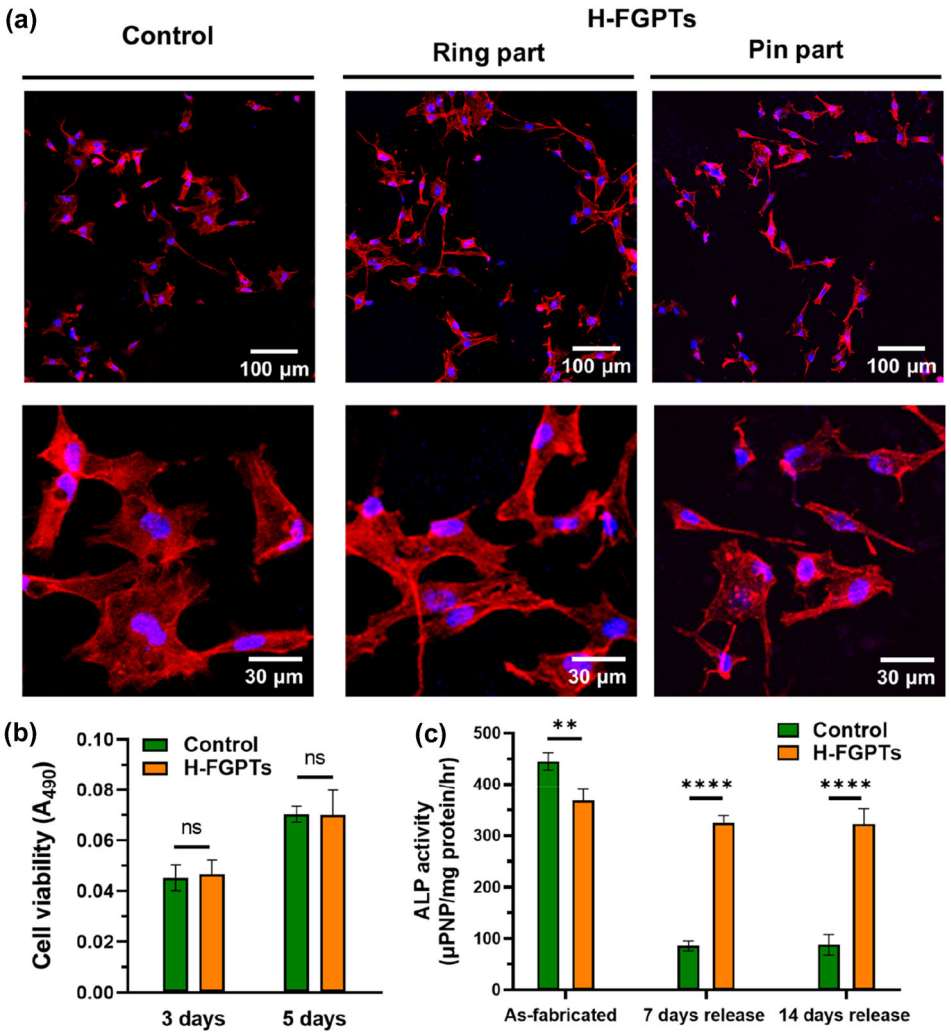

Fig. 6 **a** The observed cell morphologies of control and H-FGPTs by CLSM. **b** Cell viability measured after 3 days and 5 days of culture on each scaffold. **c** Degree of ALP activity in terms of prior release time in the control and the experimental groups (**$p < 0.01$, ****$p < 0.001$)

of embedded bolts from the grouting material reported by Thenevin et al. [55].

In terms of biomolecule release, polymeric coatings containing biomolecules have been commonly used to achieve their sustained release, which is induced by reduced diffusion rate [56, 57]. However, the application of polymeric coatings in hard-tissue scaffolds is limited by potential delamination during the implantation procedure and the unknown effect of degraded polymers under physiological conditions over a long period [58]. Thus, the densification method is a highly promising technique to gain prolonged release, as demonstrated in previous research [48, 54]. Similarly, H-FGPTs exhibited the sustained release of BMP-2, which was mainly due to the increased degree of complexity of the release pathway. This phenomenon was quantitatively assessed by first-order kinetics and by computing the relative tortuosity factor. In one study, the biological activity of loaded rhBMP-2 in the scaffolds was still maintained for 8 weeks after loading [48]. Here, the decreased rate constant inferred the prolonged release of BMP-2 from H-FGPTs. However, the release of TCH was not considerably altered in comparison with the control group. This phenomenon was in contrast to a previous article reporting the sustained release of BMP-2 and TCH [54]. As opposed to their results, the effect of outer porous ring parts on the release behavior was almost negligible due to the high porosity and large pore size of these parts [54].

In vitro cell tests were conducted to assess the biological response to the fabricated scaffolds. Firstly, the cell morphologies were observed, as demonstrated in Fig. 6a; there was no sign of cytotoxicity to preosteoblast cells. The adhered MC3T3-E1 cells exhibited extended cytoplasms with stretched filopodia. After 3 and 5 days of culture, the multiplication of cells was statistically similar between the control and H-FGPTs ($p > 0.05$). The reason for similar cell viability between the control group and H-FGPTs was due to the lower effect of BMP-2 on cell proliferation [29]. However, the trend of cell differentiation following certain periods of release greatly differed. ALP activity was higher for the control group than that for functionally graded porous Ti scaffolds due to the initial burst release. On the other hand, after

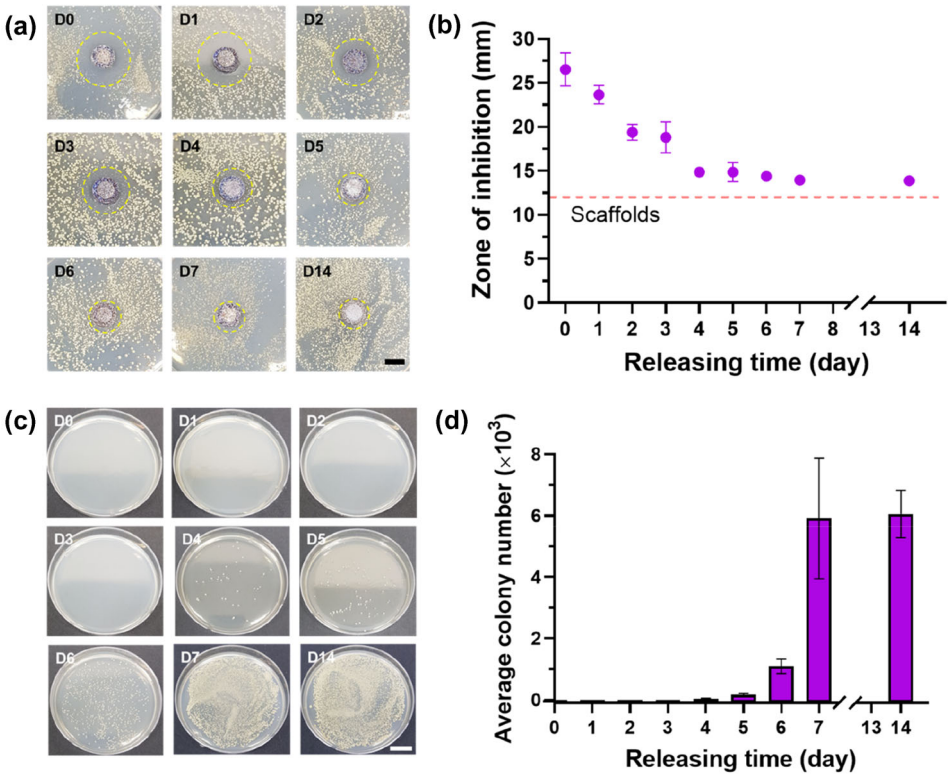

Fig. 7 **a** Optical images and **b** measured diameter of inhibition zones based on the prior release time of H-FGPTs. **c** Optical images and **d** the quantified average colony number measured diameter with different release times of H-FGPTs (the scale bar in **a** represents 10 mm and **c** represents 20 mm)

7 days of release, ALP activity dramatically decreased for the control group while it remained in the functionally graded porous Ti group. As illustrated in Fig. 5a, almost all of BMP-2 was released within 7 days for the control group, whereas certain amount of BMP-2 was still left inside the H-FGPTs. Thus, the functionally graded porous Ti scaffolds performed well in long-term application in that the osteogenic differentiation of preosteoblast cells resulted in enhanced bone regeneration. In addition, the results of in vitro antimicrobial tests demonstrated the effect of antibiotics in the early stage to prohibit acute inflammation around surgical sites; the reduced early inflammation reaction in implanted sites could alleviate the pain and discomfort. Though the antimicrobial effect was prolonged at 6 days, this duration could be further increased by adopting higher concentration of antibiotics.

The advantage of this technique lies in the assembly between the ring- and pin-shaped parts. As long as the densifying region was present, graded porous Ti scaffolds could be fabricated. As demonstrated in Fig. 8a, six different types of graded porous Ti scaffolds were produced, and the overall porosity and pore size could be altered by adjusting the diameter and height of each part. The mechanical properties of graded porous Ti scaffolds were also controllable since the mechanical properties of densified region and non-densified region are different according to the applied strain. A controlled ratio of biomolecule release could be achieved through adjusting the volumetric ratio of two parts. Moreover, numerous biomolecules including growth factors, antibiotics and functional nanoparticles could be loaded into the scaffolds in a customized manner. Considering clinical cases, conventional products with specific dimensions have been mainly utilized for surgical convenience, easy obtention, and credibility. However, individually designed grafts for the efficient healing process are necessary because the size and structure of surgical site inevitably differ among patients and bone parts. Even though titanium scaffolds made using a dynamic freeze casting method were presented in this manuscript, any of porous metallic scaffolds with ductility could be candidates for this system under a certain range of strain where severe deformation does not occur [59]. The recently developed additive manufacturing methods regarding porous metallic scaffolds achieved fair densification behaviors in scaffolds under compressive stresses [60, 61]. The porous outer layer of FGPTs is highly effective regarding bone-to-implant fixation. Since bone-related cells can infiltrate into the pores through the body fluid supply between the gap of scaffold and the surrounding bone, bone regeneration will occur inside the pores. In that manner, pores can act as starting point of bone regeneration, and the grown bones will eventually be connected to the surrounding bones (Fig. 8b). Thus, the fabricated FGPTs are highly promising as they exhibit diverse functionality regarding usable materials, a high degree of structural freedom, and the option of multiple drug delivery, which are challenging to achieve using conventional metallic scaffolds fabricated by traditional methods and recent emerging methods.

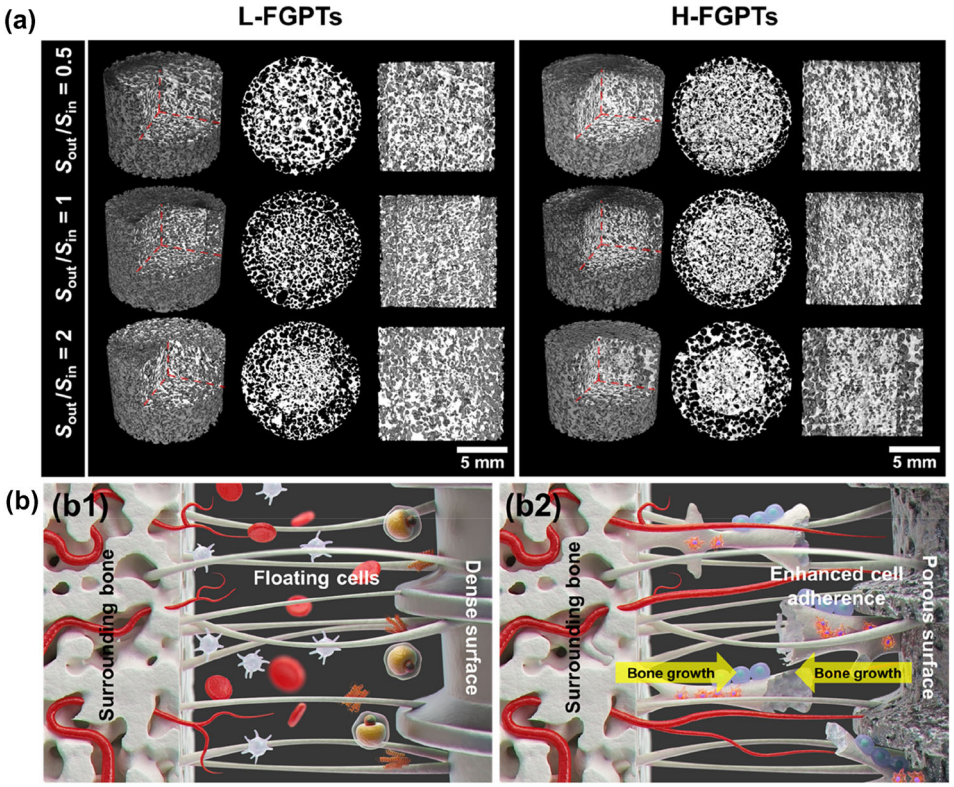

Fig. 8 **a** Micro-CT images of L-FGPTs and H-FGPTs with different S_{out}/S_{in} ratios. **b** Schematic image of bone regeneration between the scaffolds and the surrounding bone considering surface structure ((**b1**) scaffold with dense surface and (**b2**) scaffold with porous surface)

Conclusions

In this research, the assembly of two distinct porous scaffolds through a densifying process was utilized to fabricate a multiple-biomolecule delivery platform that can effectively release growth factors and antibiotics at the same time. The characteristic structure was successfully constructed and the pore characteristics were significantly changed through the densification procedure following determined theoretical calculation. As for the mechanical properties, the compressive strengths were inversely proportional to the overall porosity, but the elastic modulus was reduced due to deficient interfaces at the joint of inner and outer parts. The release behaviors of BMP-2 and TCH were monitored at pre-determined time intervals. Owing to the altered tortuosity through the densification procedure, the release of BMP-2 was prolonged in the functionally graded porous Ti scaffolds. However, TCH release was not changed in such scaffolds. The evaluation of antimicrobial properties was performed using *S. aureus* by assessing the zone of inhibition, and colony formation tests confirmed the effective termination of bacteria in a few days. The results of initial cell attachment and proliferation proved that porous Ti scaffolds with biomolecules are biocompatible, and they exhibited an enhanced maintenance of differentiation degree for FGPTs compared to the control group. In addition to the suggested structure, it is possible to fabricate scaffolds with different degrees of densification and ratio between the inner and outer parts. Therefore, versatile designs can be applied to this platform that can be tightly assembled into the targeted structure.

Acknowledgements This work was supported by the National Research Foundation of Korea (NRF) grant funded by the Korea government (MSIT) (Nos. 2021R1I1A1A01043176 and 2021R1A2C1091301), the framework of international cooperation program managed by the National Research Foundation of Korea (No. 2021K2A9A2A06037540), Korean Fund for Regenerative Medicine funded by Ministry of Science and ICT, and Ministry of Health and Welfare (No. 2021M3E5E5096420, Republic of Korea), Korea Medical Device Development Fund grant funded by the Korea government (the Ministry of Science and ICT, the Ministry of Trade, Industry and Energy, the Ministry of Health & Welfare, Republic of Korea, the Ministry of Food and Drug Safety) (Project Number: 202011B29), and the GRRC program of the Gyeo nggi Province (Grant Number GRRC-KPU2021-A01, Multi-material Machining Innovative Technology Research Center).

Author contributions HL contributed to conceptualization, investigation, validation, methodology, and writing—original draft. MKL contributed to investigation, validation, and methodology. GH contributed to validation and visualization. HEK contributed to project administration and supervision. JS and YN contributed to conceptualization and methodology. SO and CBY contributed to writing—revised draft. TSJ contributed to conceptualization, methodology, and writing—review and editing. HDJ contributed to conceptualization, methodology, writing—original draft, and writing—review and editing.

Declarations

Conflict of interest The authors declare that they have no known competing financial interests or personal relationships.

Ethical approval This article does not contain any studies with human or animal subjects performed by any of the authors.

References

1. Cheon KH, Park C, Kang MH et al (2021) Construction of tantalum/poly (ether imide) coatings on magnesium implants with both corrosion protection and osseointegration properties. Bioact Mater 6(4):1189–1200. https://doi.org/10.1016/j.bioactmat.2020.10.007
2. Jang TS, Kim DE, Han G et al (2020) Powder based additive manufacturing for biomedical application of titanium and its alloys: a review. Biomed Eng Lett 10:505–516. https://doi.org/10.1007/s13534-020-00177-2
3. Yuan L, Ding S, Wen C (2019) Additive manufacturing technology for porous metal implant applications and triple minimal surface structures: A review. Bioact Mater 4:56–70. https://doi.org/10.1016/j.bioactmat.2018.12.003
4. Kaur M, Singh K (2019) Review on titanium and titanium based alloys as biomaterials for orthopaedic applications. Mater Sci Eng C 102:844–862. https://doi.org/10.1016/j.msec.2019.04.064
5. Lee MK, Lee H, Park C et al (2022) Accelerated biodegradation of iron-based implants via tantalum-implanted surface nanostructures. Bioact Mater 9:239–250. https://doi.org/10.1016/j.bioactmat.2021.07.003
6. Yook SW, Jung HD, Park CH et al (2012) Reverse freeze casting: a new method for fabricating highly porous titanium scaffolds with aligned large pores. Acta Biomater 8(6):2401–2410. https://doi.org/10.1016/j.actbio.2012.03.020
7. Kim SW, Jung HD, Kang MH et al (2013) Fabrication of porous titanium scaffold with controlled porous structure and net-shape using magnesium as spacer. Mater Sci Eng C 33(5):2808–2815. https://doi.org/10.1016/j.msec.2013.03.011
8. Jang TS, Jung HD, Kim S et al (2017) Multiscale porous titanium surfaces via a two-step etching process for improved mechanical and biological performance. Biomed Mater 12(2):025008. https://doi.org/10.1088/1748-605X/aa5d74
9. Lee H, Jang TS, Song J et al (2016) Multi-scale porous Ti6Al4V scaffolds with enhanced strength and biocompatibility formed via dynamic freeze-casting coupled with micro-arc oxidation. Mater Lett 185:21–24. https://doi.org/10.1016/j.matlet.2016.08.075
10. Chouirfa H, Bouloussa H, Migonney V et al (2019) Review of titanium surface modification techniques and coatings for antibacterial applications. Acta Biomater 83:37–54. https://doi.org/10.1016/j.actbio.2018.10.036
11. Sarraf M, Rezvani Ghomi E, Alipour S et al (2021) A state-of-the-art review of the fabrication and characteristics of titanium and its alloys for biomedical applications. Bio-Des Manuf. https://doi.org/10.1007/s42242-021-00170-3
12. Spriano S, Yamaguchi S, Baino F et al (2018) A critical review of multifunctional titanium surfaces: new frontiers for improving osseointegration and host response, avoiding bacteria contamination. Acta Biomater 79:1–22. https://doi.org/10.1016/j.actbio.2018.08.013
13. Huang J, Zhang X, Yan W et al (2017) Nanotubular topography enhances the bioactivity of titanium implants. Nanomed: Nanotechnol Biol Med 13(6):1913–1923. https://doi.org/10.1016/j.nano.2017.03.017
14. Kim J, Lee H, Jang TS et al (2021) Characterization of titanium surface modification strategies for osseointegration enhancement. Metals 11(4):618. https://doi.org/10.3390/met11040618
15. Lee MK, Lee H, Kim HE et al (2021) Nano-topographical control of Ti-Nb-Zr alloy surfaces for enhanced osteoblastic response. Nanomaterials 11(6):1507. https://doi.org/10.3390/nano11061507
16. Yin C, Zhang T, Wei Q et al (2022) Surface treatment of 3D printed porous Ti6Al4V implants by ultraviolet photofunctionalization for improved osseointegration. Bioact Mater 7:26–38. https://doi.org/10.1016/j.bioactmat.2021.05.043
17. He Y, Li Z, Ding X et al (2022) Nanoporous titanium implant surface promotes osteogenesis by suppressing osteoclastogenesis via integrin β1/FAKpY397/MAPK pathway. Bioact Mater 8:109–123. https://doi.org/10.1016/j.bioactmat.2021.06.033
18. Kuttappan S, Mathew D, Ji Jo et al (2018) Dual release of growth factor from nanocomposite fibrous scaffold promotes vascularisation and bone regeneration in rat critical sized calvarial defect. Acta Biomater 78:36–47. https://doi.org/10.1016/j.actbio.2018.07.050
19. Lee GH, Makkar P, Paul K et al (2017) Development of BMP-2 immobilized polydopamine mediated multichannelled biphasic calcium phosphate granules for improved bone regeneration. Mater Lett 208:122–125. https://doi.org/10.1016/j.matlet.2017.05.017
20. Maher S, Kaur G, Lima-Marques L et al (2017) Engineering of micro-to nanostructured 3d-printed drug-releasing titanium implants for enhanced osseointegration and localized delivery of anticancer drugs. ACS Appl Mater Interfaces 9(35):29562–29570. https://doi.org/10.1021/acsami.7b09916
21. Sarkar N, Bose S (2020) Controlled delivery of curcumin and vitamin K2 from hydroxyapatite-coated titanium implant for enhanced in vitro chemoprevention, osteogenesis, and in vivo osseointegration. ACS Appl Mater Interfaces 12(12):13644–13656. https://doi.org/10.1021/acsami.9b22474
22. Wang C, Lai J, Li K et al (2021) Cryogenic 3D printing of dual-delivery scaffolds for improved bone regeneration with enhanced vascularization. Bioact Mater 6(1):137–145. https://doi.org/10.1016/j.bioactmat.2020.07.007
23. Bai J, Wang H, Chen H et al (2020) Biomimetic osteogenic peptide with mussel adhesion and osteoimmunomodulatory functions to ameliorate interfacial osseointegration under chronic inflammation. Biomaterials 255:120197. https://doi.org/10.1016/j.biomaterials.2020.120197
24. Qureshi AT, Doyle A, Chen C et al (2015) Photoactivated miR-148b–nanoparticle conjugates improve closure of critical size mouse calvarial defects. Acta Biomater 12:166–173. https://doi.org/10.1016/j.actbio.2014.10.010
25. Hu B, Li Y, Wang M et al (2018) Functional reconstruction of critical-sized load-bearing bone defects using a Sclerostin-targeting miR-210-3p-based construct to enhance osteogenic activity. Acta Biomater 76:275–282. https://doi.org/10.1016/j.actbio.2018.06.017
26. Xing H, Wang X, Xiao G et al (2020) Hierarchical assembly of nanostructured coating for siRNA-based dual therapy of bone regeneration and revascularization. Biomaterials 235:119784. https://doi.org/10.1016/j.biomaterials.2020.119784
27. Ständert V, Borcherding K, Bormann N et al (2021) Antibiotic-loaded amphora-shaped pores on a titanium implant surface enhance osteointegration and prevent infections. Bioact Mater 6(8):2331–2345. https://doi.org/10.1016/j.bioactmat.2021.01.012
28. Lorenzetti M, Dogša I, Stošicki T et al (2015) The influence of surface modification on bacterial adhesion to titanium-based substrates. ACS Appl Mater Interfaces 7(3):1644–1651. https://doi.org/10.1021/am507148n
29. Lee IK, Han IH, Hwang SW et al (2012) Analysis of attachment, proliferation and differentiation response of human mesenchymal stem cell to various implant surfaces coated with rhBMP-2.

J Korean Acad Prosthodont 50(1):44–52. https://doi.org/10.4047/jkap.2012.50.1.44
30. Teng F-Y, Tai IC, Ho M-L et al (2019) Controlled release of BMP-2 from titanium with electrodeposition modification enhancing critical size bone formation. Mater Sci Eng C 105:109879. https://doi.org/10.1016/j.msec.2019.109879
31. Tang W, Yu Y, Wang J et al (2020) Enhancement and orchestration of osteogenesis and angiogenesis by a dual-modular design of growth factors delivery scaffolds and 26SCS decoration. Biomaterials 232:119645. https://doi.org/10.1016/j.biomaterials.2019.119645
32. Bai L, Chen P, Zhao Y et al (2021) A micro/nano-biomimetic coating on titanium orchestrates osteo/angio-genesis and osteoimmunomodulation for advanced osseointegration. Biomaterials 278:121162. https://doi.org/10.1016/j.biomaterials.2021.121162
33. Long M, Rack HJ (1998) Titanium alloys in total joint replacement–a materials science perspective. Biomaterials 19(18):1621–1639. https://doi.org/10.1016/s0142-9612(97)00146-4
34. Sumner DR (2015) Long-term implant fixation and stress-shielding in total hip replacement. J Biomech 48(5):797–800. https://doi.org/10.1016/j.jbiomech.2014.12.021
35. Abbasian Najafabadi T, Illarionov A, Belikov S et al (2017) Metallic materials for medical use. MATEC Web Conf 132:03003. https://doi.org/10.1051/matecconf/201713203003
36. Niinomi M, Nakai M (2011) Titanium-based biomaterials for preventing stress shielding between implant devices and bone. Int J Biomater 2011:836587. https://doi.org/10.1155/2011/836587
37. Vijayavenkataraman S, Gopinath A, Lu WF (2020) A new design of 3D-printed orthopedic bone plates with auxetic structures to mitigate stress shielding and improve intra-operative bending. Bio-Des Manuf 3(2):98–108. https://doi.org/10.1007/s42242-020-00066-8
38. Jung HD, Yook SW, Han CM et al (2014) Highly aligned porous Ti scaffold coated with bone morphogenetic protein-loaded silica/chitosan hybrid for enhanced bone regeneration. J Biomed Mater Res Part B 102(5):913–921. https://doi.org/10.1002/jbm.b.33072
39. Bari K, Arjunan A (2019) Extra low interstitial titanium based fully porous morphological bone scaffolds manufactured using selective laser melting. J Mech Behav Biomed Mater 95:1–12. https://doi.org/10.1016/j.jmbbm.2019.03.025
40. Caparros C, Ortiz-Hernandez M, Molmeneu M et al (2016) Bioactive macroporous titanium implants highly interconnected. J Mater Sci-Mater Med 27(10):151. https://doi.org/10.1007/s10856-016-5764-8
41. Wang C, Chen H, Zhu X et al (2017) An improved polymeric sponge replication method for biomedical porous titanium scaffolds. Mater Sci Eng C 70(Pt 2):1192–1199. https://doi.org/10.1016/j.msec.2016.03.037
42. Lee JB, Ahn MK, Koh YH et al (2016) Ti scaffolds with tailored porosities and mechanical properties using porous polymer templates. Mater Des 101:323–331. https://doi.org/10.1016/j.matdes.2016.03.142
43. Taniguchi N, Fujibayashi S, Takemoto M et al (2016) Effect of pore size on bone ingrowth into porous titanium implants fabricated by additive manufacturing: an in vivo experiment. Mater Sci Eng C 59:690–701. https://doi.org/10.1016/j.msec.2015.10.069
44. Jonitz-Heincke A, Wieding J, Schulze C et al (2013) Comparative analysis of the oxygen supply and viability of human osteoblasts in three-dimensional titanium scaffolds produced by laser-beam or electron-beam melting. Materials 6(11):5398–5409. https://doi.org/10.3390/ma6115398
45. Schouman T, Schmitt M, Adam C et al (2016) Influence of the overall stiffness of a load-bearing porous titanium implant on bone ingrowth in critical-size mandibular bone defects in sheep. J Mech Behav Biomed Mater 59:484–496. https://doi.org/10.1016/j.jmbbm.2016.02.036
46. Lou S, Pagani L, Zeng W et al (2019) Surface texture evaluation of additively manufactured metallic cellular scaffolds for acetabular implants using X-ray computed tomography. Bio-Des Manuf 2(2):55–64. https://doi.org/10.1007/s42242-019-00042-x
47. Vilardell AM, Cinca N, Garcia-Giralt N et al (2018) In-vitro study of hierarchical structures: anodic oxidation and alkaline treatments onto highly rough titanium cold gas spray coatings for biomedical applications. Mater Sci Eng C 91:589–596. https://doi.org/10.1016/j.msec.2018.05.071
48. Jung HD, Jang TS, Wang L et al (2015) Novel strategy for mechanically tunable and bioactive metal implants. Biomaterials 37:49–61. https://doi.org/10.1016/j.biomaterials.2014.10.027
49. Jung HD, Lee H, Kim HE et al (2015) Fabrication of mechanically tunable and bioactive metal scaffolds for biomedical applications. J Vis Exp 106:e53279. https://doi.org/10.3791/53279
50. Dong XN, Acuna RL, Luo Q et al (2012) Orientation dependence of progressive post-yield behaviour of human cortical bone in compression. J Biomech 45(16):2829–2834. https://doi.org/10.1016/j.jbiomech.2012.08.034
51. Wenzel RP (2010) Minimizing surgical-site infections. N Engl J Med 362(1):75–77. https://doi.org/10.1056/NEJMe0908753
52. Wenke JC, Guelcher SA (2011) Dual delivery of an antibiotic and a growth factor addresses both the microbiological and biological challenges of contaminated bone fractures. Expert Opin Drug Deliv 8(12):1555–1569. https://doi.org/10.1517/17425247.2011.628655
53. Radda'a NS, Goldmann WH, Detsch R et al (2017) Electrophoretic deposition of tetracycline hydrochloride loaded halloysite nanotubes chitosan/bioactive glass composite coatings for orthopedic implants. Surf Coat Tech 327:146–157. https://doi.org/10.1016/j.surfcoat.2017.07.048
54. Lee H, Lee MK, Cheon KH et al (2021) Functionally assembled metal platform as lego-like module system for enhanced mechanical tunability and biomolecules delivery. Mater Des 207:109840. https://doi.org/10.1016/j.matdes.2021.109840
55. Thenevin I, Blanco-Martín L, Hadj-Hassen F et al (2017) Laboratory pull-out tests on fully grouted rock bolts and cable bolts: Results and lessons learned. J Rock Mech Geotech Eng 9(5):843–855. https://doi.org/10.1016/j.jrmge.2017.04.005
56. Min J, Braatz RD, Hammond PT (2014) Tunable staged release of therapeutics from layer-by-layer coatings with clay interlayer barrier. Biomaterials 35(8):2507–2517. https://doi.org/10.1016/j.biomaterials.2013.12.009
57. Chung RJ, Ou KL, Tseng WK et al (2016) Controlled release of BMP-2 by chitosan/γ-PGA polyelectrolyte multilayers coating on titanium alloy promotes osteogenic differentiation in rat bone-marrow mesenchymal stem cells. Surf Coat Tech 303:283–288. https://doi.org/10.1016/j.surfcoat.2016.03.081
58. Barfeie A, Wilson J, Rees J (2015) Implant surface characteristics and their effect on osseointegration. Br Dent J 218(5):E9. https://doi.org/10.1038/sj.bdj.2015.171
59. Jung HD, Yook SW, Jang TS et al (2013) Dynamic freeze casting for the production of porous titanium (Ti) scaffolds. Mater Sci Eng C 33(1):59–63. https://doi.org/10.1016/j.msec.2012.08.004
60. Bobbert FSL, Lietaert K, Eftekhari AA et al (2017) Additively manufactured metallic porous biomaterials based on minimal surfaces: a unique combination of topological, mechanical, and mass transport properties. Acta Biomater 53:572–584. https://doi.org/10.1016/j.actbio.2017.02.024
61. Li Y, Jahr H, Lietaert K et al (2018) Additively manufactured biodegradable porous iron. Acta Biomater 77:380–393. https://doi.org/10.1016/j.actbio.2018.07.011